Journal of Materials Chemistry A

ROYAL SOCIETY OF CHEMISTRY

PAPER

View Article Online
View Journal | View Issue

Cite this: J. Mater. Chem. A, 2024, 12, 24977

Co-deposition of conductive additives and lithium peroxide during discharge to boost the performance of lithium–oxygen batteries†

Yu-Long Liang,‡[ab] Yue Yu,‡[c] Zi-Wei Li,[ab] Jin Wang,[b] Jun-Min Yan,[a] Gang Huang*[b] and Xin-Bo Zhang*[b]

Received 12th June 2024
Accepted 29th July 2024

DOI: 10.1039/d4ta04077e

rsc.li/materials-a

Lithium–oxygen batteries (LOBs) have been regarded as a promising energy storage system for applications in electric vehicles and aviation. However, the development of high-performance LOBs has been hindered by the challenges associated with insulating discharge products, such as low energy efficiency and poor rate performance. Here, we report that insulating lithium peroxide (Li_2O_2) can deposit with a carbon nanotube (CNT) additive during the discharge process and eventually be woven into a conductive network. The constructed network enhances the conductivity of Li_2O_2 and accelerates the kinetics of electrode reactions. As a result, the battery containing 1.0 mg mL^{-1} CNTs in the electrolyte exhibits a high areal capacity of 5.7 mA h cm^{-2} and superior rate performance at 1.41 A g_{CNT}^{-1}. Furthermore, the introduction of ruthenium nanoparticles to the CNTs results in stable cycling for 550 hours. This research opens up a new avenue for addressing the issues caused by insulating discharge products in LOBs.

Introduction

Among the alternatives to conventional Li-ion batteries (LIBs), aprotic lithium–oxygen batteries (LOBs) have triggered worldwide interest due to their high energy density of ~3500 W h kg^{-1}.[1–3] Nevertheless, the practical applications of LOBs are likely to be impeded by their low practical capacity, large voltage hysteresis, and poor rate performance.[4] An essential factor contributing to these drawbacks is the inherently insulating nature of the discharge product.[5–7] Therefore, as one of the solutions, it is of great significance to enhance the electron transfer within the discharge products. In LOBs, two approaches have generally been employed for this purpose. One involves increasing the proportion of defect-rich or amorphous components in the most common discharge product, Li_2O_2. Existing research studies have demonstrated that the conductivity of defect-rich Li_2O_2 or amorphous Li_2O_2 is significantly higher than that of the crystalline one,[8–10] especially at the surface.[11,12] Another approach involves employing catalysts to facilitate battery cycling based on chemicals with higher conductivity, such as LiO_2.[13–16] Despite the enhancement in the conductivity of discharge products achieved by the above two approaches, the conductivity has not yet reached satisfactory levels.[9] To date, it still remains a challenge to find effective ways to enhance the conductivity of discharge products.

Introducing conductive components into insulating electrode materials has demonstrated some success in LIBs. The most notable example is the carbon coating of lithium iron phosphate ($LiFePO_4$), which makes it an ideal battery material for large-scale energy storage and electric vehicle applications.[17] The method of electrochemically synthesizing composites of nanoparticles and substrates has been widely reported in the field of electrodeposition. Nanoparticles embedded in coatings could impart various functions to the coating, such as wear resistance, self-cleaning, and biocompatibility.[18–20]

Here, we have introduced carbon nanotubes (CNTs) as a kind of electrolyte additive, with the intention of weaving the insulating discharge product Li_2O_2 into a conductive network. The constructed network enhances the conductivity of Li_2O_2 and accelerates the kinetics of electrode reactions. Experiments demonstrate that the CNTs can co-deposit with Li_2O_2, and the percolation threshold of CNTs for significantly improving the conductivity is approximately 3 wt%, which is consistent with the theoretical calculation results. A concentration of 10 wt% CNTs in the Li_2O_2/CNTs mixture results in a conductivity of 8.26×10^{-3} S cm^{-1}, indicating that the strategy reported here can enhance the conductivity of Li_2O_2 without significantly reducing the energy density of LOBs. Due to the co-deposition of CNTs and Li_2O_2, the LOBs exhibit a fivefold slower increase in charge transfer resistance (R_{ct}) than the batteries without CNTs,

[a]Department of Materials Science and Engineering, Key Laboratory of Automobile Materials, Ministry of Education, Jilin University, Changchun 130022, China
[b]State Key Laboratory of Rare Earth Resource Utilization, Changchun Institute of Applied Chemistry, Chinese Academy of Sciences, Changchun 130022, China. E-mail: ghuang@ciac.ac.cn; xbzhang@ciac.ac.cn
[c]Department of Chemistry and Waterloo Institute for Nanotechnology, University of Waterloo, Ontario N2L 3G1, Canada

† Electronic supplementary information (ESI) available. See DOI: https://doi.org/10.1039/d4ta04077e

‡ Yu-Long Liang and Yue Yu contributed equally to this work.

a large discharge capacity of 5.7 mA h cm^{-2}, and superior high-rate performance at 1.41 A g_{CNT}^{-1}. Furthermore, by loading ruthenium nanoparticles onto the CNTs, the battery ultimately achieves a satisfactory cycle life of about 550 h.

Results and discussion

Compared to metal nanoparticles, carbon-based materials are lighter and more stable in LOBs. Therefore, three kinds of carbon materials—CNTs, Ketjen black (KB), and Super P (SP) were selected as conductive electrolyte additives to test their ability to co-deposit with Li_2O_2. To enhance the dispersion of these carbon materials, sodium dodecyl benzene sulfonate (SDBS) was chosen as the surfactant and added to the electrolyte along with the carbon materials. Due to its large organic branch chain, SDBS has acceptable solubility in the tetraethylene glycol dimethyl ether (TEGDME) solution. Additionally, the benzene ring on the branch chain can bind to the carbon materials through π–π interaction to improve their dispersion in the electrolyte.[21,22] The cyclic voltammetry (CV) test conducted in an oxygen atmosphere demonstrates that SDBS remains stable in the harsh LOB working environment (Fig. S1†).

Compared to the toroid discharge products in the batteries without conductive additives (Fig. 1a and b), it is obvious that the CNTs intertwine with the discharge products, and some CNTs even embed into Li_2O_2 (Fig. 1c and d). The addition of KB results in the formation of conformal discharge products, as shown in Fig. 1e and f. In contrast, SP only loosely mixes with Li_2O_2 (Fig. 1g and h). When testing the discharge performance of LOBs with and without conductive electrolyte additives, it is evident that the battery with CNTs exhibits the highest capacity and the lowest discharge overpotential among all the LOBs (Fig. 2a). Therefore, CNTs were chosen as the optimal electrolyte additive for further study.

The experiment depicted in Fig. 2b explored the effect of CNT content on the battery discharge performance. The discharge capacity increases with an increase in CNT content up to 1.0 mg mL^{-1}, reaching the highest discharge capacity of 5.7 mA h cm^{-2}, which is twice that of the battery with 0.2 mg mL^{-1} CNTs (2.57 mA h cm^{-2}). Besides, increasing CNT content also decreases the discharge overpotential, which is likely caused by the higher CNT content providing a larger electrochemical active surface area. When the CNT content exceeds

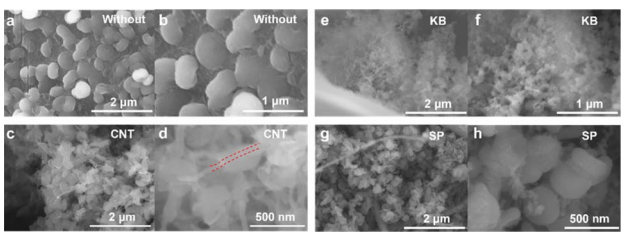

Fig. 1 Scanning electron microscope (SEM) images of the cathodes discharged to 2 V at 0.1 mA cm^{-2}. (a and b) Without a conductive additive. (c and d) With 3 mg mL^{-1} CNTs. (e and f) With 3 mg mL^{-1} KB. (g and h) With 3 mg mL^{-1} SP.

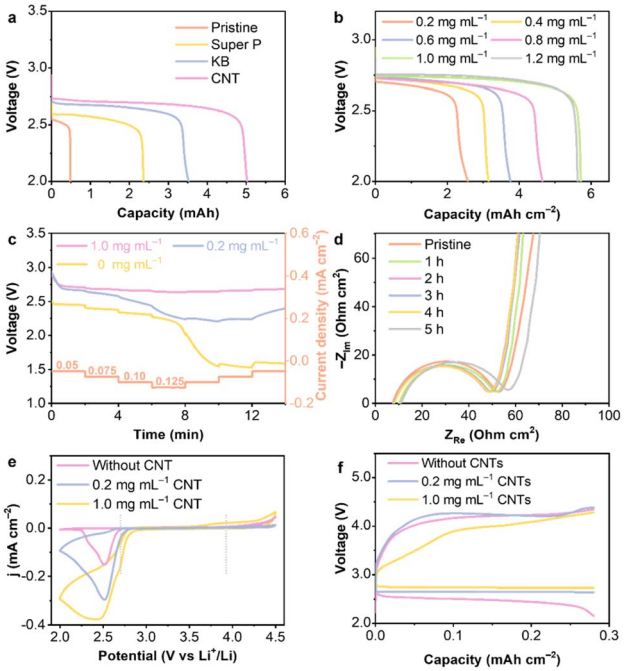

Fig. 2 (a) Discharge curves of LOBs with and without different conductive additives (current density: 0.1 mA cm^{-2}). (b) Discharge capacities of LOBs with various CNT contents ranging from 0.2 to 1.2 mg mL^{-1} at 0.1 mA cm^{-2}. (c) Rate performance of LOBs with 0, 0.2, and 1.0 mg mL^{-1} CNTs. (d) EIS curves of LOBs with 1.0 mg mL^{-1} CNTs discharged for 1 to 5 hours at 0.05 mA cm^{-2}. (e) CV curves of LOBs with 0, 0.2, and 1.0 mg mL^{-1} CNTs (scan rate: 0.1 mV s^{-1}). (f) The first discharge and charge curves of batteries with 0, 0.2, and 1.0 mg mL^{-1} CNTs (current density: 0.1 mA cm^{-2}).

1.0 mg mL^{-1}, the discharge capacity exhibits a decrease phenomenon. This can be attributed to the high concentration causing the CNTs to aggregate together. As a result, it becomes harder for them to move freely and deposit with Li_2O_2. This view can be supported by Fig. S2,† where the CNTs aggregate more rapidly at 1.2 mg mL^{-1} than at 1.0 mg mL^{-1}. It should be mentioned that the electrolyte used in each cell is 100 μL, containing 0.1 mg CNTs (for 1.0 mg mL^{-1}). To illustrate the superiority brought by the CNT additive, we also sprayed 0.1 mg CNTs on carbon paper (CP) and tested the discharge capacity of LOBs. As shown in Fig. S3,† the capacity is only 0.64 mA h cm^{-2}, much lower than the 5.7 mA h cm^{-2} delivered by the batteries with the CNT additive. Fig. 2c compares the rate performance of batteries with 0, 0.2, and 1.0 mg mL^{-1} CNTs. Only the battery with 1.0 mg mL^{-1} CNTs can return to its initial state after discharging at a maximum current density of 0.125 mA cm^{-2}, equivalent to 1.41 A g_{CNT}^{-1} based on the mass of the active material, highlighting the effectiveness of the CNT additive in boosting the rate capability of LOBs.

In typical LOBs, the accumulation of insulating discharge products will passivate the cathode, leading to a rapid increase in charge transfer resistance (R_{ct}).[23] However, with the method developed here, the growth of R_{ct} will be much slower, as the CNTs could continuously connect to the cathode and remain exposed to the electrolyte. To confirm this, electrochemical

impedance spectroscopy (EIS) measurement was conducted. Fig. 2d and S4† present the EIS curves of LOBs with 1.0 mg mL^{-1} CNTs and without CNTs at various states of discharge. All EIS plots exhibit a typical semicircular shape followed by a diffusion line. The diameter of the semicircle in the middle frequency represents the R_{ct}. The R_{ct} of the battery with CNTs changes from 41 Ω (initial) to 47 Ω (after 5 hours of discharge), while the R_{ct} of the battery without CNTs rapidly increases from 39 Ω (initial) to 71 Ω (after 5 hours of discharge). These results provide solid evidence that the CNTs co-deposit with Li_2O_2. In addition, Fig. S5† presents the EIS curves of the LOB with 1.0 mg mL^{-1} CNTs before and after being discharged to 2 V. The small increase in R_{ct} indicates that the sudden death of LOBs should not be simply attributed to the charge transfer impedance.[23]

The CV experiment provides further evidence that the CNTs co-deposit with Li_2O_2 (Fig. 2e). The battery with 1.0 mg mL^{-1} CNTs exhibits a higher onset reduction potential (2.86 V) compared to the batteries with 0.2 mg mL^{-1} CNTs (2.77 V) and without CNTs (2.68 V). Additionally, the shape of the CV curve for the battery with 0.2 mg mL^{-1} CNTs closely resembles that of the battery without CNTs, except for a larger current response. In contrast, for the battery with 1.0 mg mL^{-1} CNTs, an additional reduction peak at 2.69 V (left dashed line) and an additional oxidation peak at around 3.85 V appear, consistent with the first discharge and charge curves shown in Fig. 2f. The battery with 1.0 mg mL^{-1} CNTs exhibits a higher discharge plateau and a lower charge potential (around 3.9 V). The reduced charge overpotential should not solely be attributed to the decomposition of Li_2O_2 promoted by the CNT surface, because the charge potential of the battery with 0.2 mg mL^{-1} CNTs shows no significant change compared to the battery without CNTs. The appearance of the two additional peaks in Fig. 2e and the change in charging voltage in Fig. 2f may be attributed to the amount of co-deposited CNTs in these batteries reaching the percolation threshold.

Percolation theory is well suited to describe the conductivity of the mixture of CNTs and Li_2O_2 reported here.[24–26] According to the percolation theory, a percolation threshold exists. Below this threshold, a giant connected component would not form. Above this threshold, a giant component connects the boundaries, resulting in significantly improved conductivity.[27] To describe the percolation behaviour of this system and determine the approximate percolation threshold, CNTs of different mass percentages were uniformly mixed with commercial Li_2O_2. Subsequently, the mixtures were compressed into samples. Before testing electronic conductivity, a layer of silver paste was applied to the ends of these samples. Fig. 3a and b display the digital photographs of the samples, and Fig. 3c depicts their conductivity. Specific data are listed in Table S1.† The conductivity of pure Li_2O_2 is only 1.50×10^{-11} S cm^{-1}, closely matching the reported data in the literature.[28] The conductivity increases rapidly with the increase in CNT content. At 10 wt%, the conductivity reaches 8.26×10^{-3} S cm^{-1}, significantly higher than the conductivity predicted for defect-rich and amorphous Li_2O_2.[8–10] This indicates that the problems caused by insulating Li_2O_2 can be alleviated by just introducing CNTs into the electrolyte.

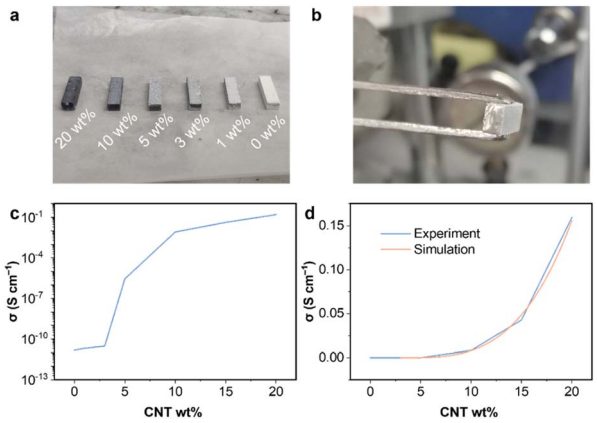

Fig. 3 (a) Optical images of Li_2O_2 samples mixed with different amounts of CNTs. (b) The end face of a sample that is covered with silver paste. (c) Relationship between the conductivity and the CNT content. (d) Comparison curves of the experimental and calculated conductivities.

The conductivity variation with respect to the CNT content was also simulated using a percolation model (Fig. S6–S9†). The percolation threshold obtained here, approximately 3 wt%, aligns with the result presented in Fig. 3c. The conductivity of Li_2O_2 shows almost no change at low CNT content (from 1 wt% to 3 wt%). As shown in Fig. 3d, the conductivity of Li_2O_2/CNTs was calculated using the Kirkpatrick–Zallen model and compared with the experimental values. As shown in eqn (1), σ represents the conductivity of the mixture, σ_p represents the conductivity of the filler (obtained by testing the 100 wt% CNT sample), v represents the content of the filler, v_c represents the content of the percolation threshold, and x represents the coefficients related to the dimensions of the system.[29] The good agreement between the two datasets demonstrates the validity of using the percolation model for this kind of analysis. Fig. S7† shows the SEM image of the sample containing 10 wt% CNTs, where CNTs are tightly entangled with Li_2O_2. The similarity between the mechanically mixed sample and the co-deposited sample during discharge (Fig. 1a and b) suggests that the conductivity of the co-deposited sample is also enhanced.

$$\sigma = \sigma_p (v - v_c)^x \quad (1)$$

SEM images of the cathodes after the first discharge and charge processes are captured to illustrate the functions of CNTs. As shown in Fig. 4a and b, during discharging, large amounts of CNTs entangle with Li_2O_2, and some CNTs even embed into Li_2O_2 (highlighted by the red dotted line in Fig. 4a). In LOBs with CNTs as the cathodes, the discharge products are typically localized very close to the cathode side.[30,31] However, for the batteries reported here, Li_2O_2 tends to continue stacking on the surface of the cathode. After the subsequent charge process, no significant Li_2O_2 can be observed on the cathode surface (Fig. 4c and d). Also, most of the deposited CNTs return to the electrolyte, while only a few CNTs still agglomerate and remain on the cathode surface (Fig. S10†). Fig. 4e schematically illustrates the possible discharge process enabled by the CNT

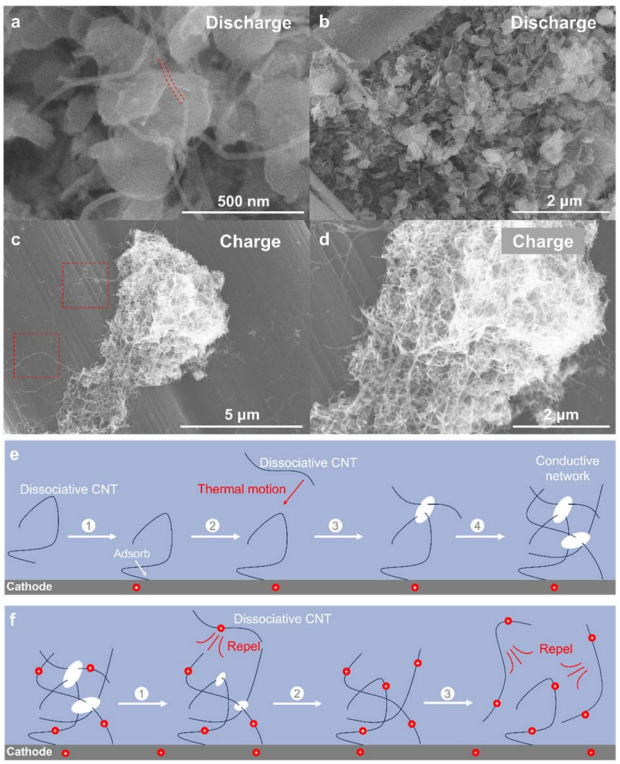

Fig. 4 SEM images of the cathodes of LOBs with 1.0 mg mL^{-1} CNTs after the first (a and b) discharge and (c and d) charge processes. A schematic illustration of the function of CNTs in the (e) discharge and (f) charge processes.

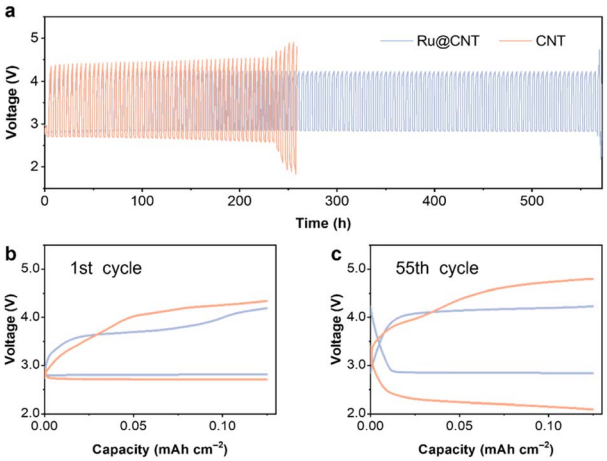

Fig. 5 (a) Cycle performance of LOBs with CNTs or Ru@CNT additive (CNT content: 1.0 mg mL^{-1}, current density: 0.05 mA cm^{-2}, and areal capacity: 0.125 mA h cm^{-2}). The discharge and charge curves of the (b) 1st cycle and (c) 55th cycle.

additives. The first step involves the adsorption of CNTs on the CP surface. As depicted in Fig. 4c, some CNTs are tightly adsorbed to the surface of the cathode, likely due to the π–π interaction between the CNTs and CP surface.[32] For the dissociated CNTs, they could approach the cathode surface through thermal motion. Subsequently, Li_2O_2 preferentially grows on the surface of CNTs, because the discharge potential of batteries with CNTs is higher than that of batteries without CNTs. As the discharge progresses, the Li_2O_2 grown on the surface of CNTs could connect the adjacent CNTs and eventually be woven into a conductive network. During the charge process (Fig. 4f), the continuous decomposition of Li_2O_2 leads to the deconstruction of the conductive network. Electrostatic repulsion primarily influences this process[33] and would become more significant during charge due to the higher potential of the cathode, which results in more positive charges on the surfaces of CNTs and the cathode. This is because the cathode has a higher potential during charge, which leads to more positive charges at the surfaces of CNTs and the cathode.[34]

Cycling performance is crucial for rechargeable batteries. However, as shown in Fig. 5a, the battery with 1.0 mg mL^{-1} CNTs could only maintain steady operation for about 250 hours. This poor cycling performance is mainly attributed to the sluggish reaction kinetics of the CP cathode without catalysts and the detachment of CNTs from the cathode before complete oxidation of Li_2O_2.[35,36] To improve cycling performance, ruthenium-decorated carbon nanotubes (Ru@CNTs) were prepared as the electrolyte additive for further investigation,[37] since metals and metal oxides are often used as catalysts to improve the electrochemical performance of LOBs.[38–40] The transmission electron microscopy (TEM) image shows that the diameter of the ruthenium particles on the surface of CNTs is approximately 5 nm (Fig. S11†). High resolution transmission electron microscope image (HRTEM, inset of Fig. S11†), XRD patterns (Fig. S12†), and X-ray photoelectron spectroscopy spectra (XPS, Fig. S13†) all confirm the presence of ruthenium particles. Due to the improved catalytic activity enabled by ruthenium particles, the battery with 1.0 mg mL^{-1} Ru@CNT exhibits lower overpotential in both the charge and discharge processes (Fig. 5b and c) and a much longer cycle life of 550 hours. Additionally, as revealed by the XRD patterns of the cathodes at different states (Fig. S14†), the battery follows the typical Li–O_2 electrochemistry with highly reversible formation and decomposition of Li_2O_2.

Conclusions

In summary, we have developed a simple but effective method of introducing CNTs as the additive into the electrolyte to alleviate the shortcomings brought by insulating Li_2O_2. With the assistance of CNTs, Li_2O_2 can connect adjacent CNTs and ultimately weave the CNTs into a conductive network, enhancing the conductivity of Li_2O_2. The battery with 1.0 mg mL^{-1} CNTs in the electrolyte exhibits a high capacity of 5.7 mA h cm^{-2} and superior rate performance at 1.41 A g_{CNT}^{-1}. This performance improvement can be attributed to the reduced passivation of the cathode induced by the co-deposition of CNTs and Li_2O_2. This viewpoint is supported by the fact that the existence of the CNT additive decreases the increase rate of R_{ct} by five times. Moreover, both the experimental and calculated results indicate that the conductivity of Li_2O_2 begins to increase when it contains approximately 3 wt% CNTs, reaching 8.26 ×

10^{-3} S cm^{-1} with 10 wt% CNTs. Besides, by incorporating ruthenium nanoparticles onto the CNTs, the battery ultimately achieves a satisfactory cycle life of about 550 hours. This study proposes a new strategy for enhancing the conductivity of discharge products to boost the performance of LOBs.

Data availability

The data supporting this article have been included as part of the ESI.†

Author contributions

Yu-Long Liang and Yue Yu: writing – original draft, data curation, methodology. Zi-Wei Li, Jin Wang, and Jun-Min Yan: data analysis. Gang Huang and Xin-Bo Zhang: supervision, writing – review & editing.

Conflicts of interest

The authors declare that they have no competing financial interests or personal relationships that could have appeared to influence the work reported in this paper.

Acknowledgements

This work was financially supported by the National Key R&D Program of China (2021YFF0500600), National Natural Science Foundation of China (U23A20575, U22A20437, and 52171194), New Cornerstone Science Foundation through the XPLORER PRIZE, CAS Project for Young Scientists in Basic Research (YSBR-058), and National Natural Science Foundation of China Outstanding Youth Science Foundation of China (Overseas).

References

1 S. Xing, Z. Zhang, Y. Dou, M. Li, J. Wu, Z. Zhang and Z. Zhou, *CCS Chem.*, 2023, **6**, 1810–1820.
2 Y. Zhang, Z. Gou, K. Zheng, Y. Dou and Z. Zhou, *J. Phys. Chem. Lett.*, 2024, **15**, 6598–6604.
3 Y. Dou, S. Xing, Z. Zhang and Z. Zhou, *Electrochem. Energy Rev.*, 2024, **7**, 6.
4 T. Liu, J. P. Vivek, E. W. Zhao, J. Lei, N. Garcia-Araez and C. P. Grey, *Chem. Rev.*, 2020, **120**, 6558–6625.
5 X. Zhang, P. Dong, S. Noh, X. Zhang, Y. Cha, S. Ha, J. H. Jang and M. K. Song, *Angew. Chem., Int. Ed.*, 2022, **62**, e202212942.
6 L. Su, Y. Zhang, X. Zhan, L. Zhang, Y. Zhao, X. Zhu, H. Wu, H. Chen, C. Shen and L. Wang, *ACS Appl. Mater. Interfaces*, 2022, **14**, 40975–40984.
7 Y. Ko, H. Park, K. Lee, S. J. Kim, H. Park, Y. Bae, J. Kim, S. Y. Park, J. E. Kwon and K. Kang, *Angew. Chem., Int. Ed.*, 2020, **59**, 5376–5380.
8 R. Gao, X. Liang, P. Yin, J. Wang, Y. L. Lee, Z. Hu and X. Liu, *Nano Energy*, 2017, **41**, 535–542.
9 F. Tian, M. D. Radin and D. J. Siegel, *Chem. Mater.*, 2014, **26**, 2952–2959.
10 O. Gerbig, R. Merkle and J. Maier, *Adv. Mater.*, 2013, **25**, 3129–3133.
11 M. D. Radin, J. F. Rodriguez, F. Tian and D. J. Siegel, *J. Am. Chem. Soc.*, 2012, **134**, 1093–1103.
12 D. Zhai, H. H. Wang, J. Yang, K. C. Lau, K. Li, K. Amine and L. A. Curtiss, *J. Am. Chem. Soc.*, 2013, **135**, 15364–15372.
13 A. Halder, A. T. Ngo, X. Luo, H. H. Wang, J. G. Wen, P. Abbasi, M. Asadi, C. Zhang, D. Miller, D. Zhang, J. Lu, P. C. Redfern, K. C. Lau, R. Amine, R. S. Assary, Y. J. Lee, A. Salehi-Khojin, S. Vajda, K. Amine and L. A. Curtiss, *J. Phys. Chem. A*, 2019, **123**, 10047–10056.
14 A. Halder, H.-H. Wang, K. C. Lau, R. S. Assary, J. Lu, S. Vajda, K. Amine and L. A. Curtiss, *ACS Energy Lett.*, 2018, **3**, 1105–1109.
15 J. Lu, Y. Jung Lee, X. Luo, K. Chun Lau, M. Asadi, H.-H. Wang, S. Brombosz, J. Wen, D. Zhai, Z. Chen, D. J. Miller, Y. Sub Jeong, J.-B. Park, Z. Zak Fang, B. Kumar, A. Salehi-Khojin, Y.-K. Sun, L. A. Curtiss and K. Amine, *Nature*, 2016, **529**, 377–382.
16 C. Zhang, S. Wang, T. Yang, N. Shan, S. K. Singh, A. Jaradat, M. K. Ncube, P. Redfern, A. Subramanian, Z. Huang, A. T. Ngo, L. A. Curtiss and A. Salehi-khojin, *Energy Storage Mater.*, 2023, **60**, 102844.
17 J. Wang and X. Sun, *Energy Environ. Sci.*, 2015, **8**, 1110–1138.
18 M. Musiani, *Electrochim. Acta*, 2000, **45**, 3397–3402.
19 A. Lelevic and F. C. Walsh, *Surf. Coat. Technol.*, 2019, **378**, 124803.
20 F. C. Walsh, S. Wang and N. Zhou, *Curr. Opin. Electrochem.*, 2020, **20**, 8–19.
21 E. H. Joo, T. Kuila, N. H. Kim, J. H. Lee, S. A. Kim, E. G. Park and U. H. Lee, *Adv. Mater. Res.*, 2013, **747**, 246–249.
22 X. Yan, X. Zhang, H. Liu, Y. Liu, J. Ding, Y. Liu, Q. Cai and J. Zhang, *Synth. Met.*, 2014, **196**, 1–7.
23 Z. Zhang, X. Xiao, W. Yu, Z. Zhao and P. Tan, *Nano Lett.*, 2022, **22**, 7527–7534.
24 G. Pike and C. Seager, *Phys. Rev. B: Solid State*, 1974, **10**, 1421.
25 K. Kalaitzidou, H. Fukushima and L. T. Drzal, *Materials*, 2010, **3**, 1089–1103.
26 N. A. M. Radzuan, A. B. Sulong and J. Sahari, *Int. J. Hydrogen Energy*, 2017, **42**, 9262–9273.
27 D. Stauffer and A. Aharony, *Introduction to Percolation Theory*, Taylor & Francis, 2018.
28 B. D. Adams, C. Radtke, R. Black, M. L. Trudeau, K. Zaghib and L. F. Nazar, *Energy Environ. Sci.*, 2013, **6**, 1772–1778.
29 D. Liu, J. Wang, W. Peng, H. Wang and H. Ren, *Compos. Sci. Technol.*, 2022, **221**, 109300.
30 L. Carbone, P. T. Moro, M. Gobet, S. Munoz, M. Devany, S. G. Greenbaum and J. Hassoun, *ACS Appl. Mater. Interfaces*, 2018, **10**, 16367–16375.
31 X. Huang, H. Yu, H. Tan, J. Zhu, W. Zhang, C. Wang, J. Zhang, Y. Wang, Y. Lv, Z. Zeng, D. Liu, J. Ding, Q. Zhang, M. Srinivasan, P. M. Ajayan, H. H. Hng and Q. Yan, *Adv. Funct. Mater.*, 2014, **24**, 6516–6523.
32 D.-Q. Yang, J.-F. Rochette and E. Sacher, *J. Phys. Chem. B*, 2005, **109**, 4481–4484.
33 F. Walsh and C. Ponce de Leon, *Trans. IMF*, 2014, **92**, 83–98.

34 A. J. Bard, L. R. Faulkner and H. S. White, *Electrochemical Methods: Fundamentals and Applications*, John Wiley & Sons, New York, 2022.
35 L. N. Song, W. Zhang, Y. Wang, X. Ge, L. C. Zou, H. F. Wang, X. X. Wang, Q. C. Liu, F. Li and J. J. Xu, *Nat. Commun.*, 2020, **11**, 2191.
36 X. Wang, C. Pei, Q. Wang, W. Ge, J. Huo and S. Guo, *Appl. Surf. Sci.*, 2021, **558**, 149888.
37 Q. C. Liu, L. Li, J. J. Xu, Z. W. Chang, D. Xu, Y. B. Yin, X. Y. Yang, T. Liu, Y. S. Jiang, J. M. Yan and X. B. Zhang, *Adv. Mater.*, 2015, **27**, 8095–8101.
38 Y. Gong, W. Ding, Z. Li, R. Su, X. Zhang, J. Wang, J. Zhou, Z. Wang, Y. Gao and S. Li, *ACS Catal.*, 2018, **8**, 4082–4090.
39 X. Zhang, Y. Gong, S. Li and C. Sun, *ACS Catal.*, 2017, **7**, 7737–7747.
40 X. Hu, G. Luo, Q. Zhao, D. Wu, T. Yang, J. Wen, R. Wang, C. Xu and N. Hu, *J. Am. Chem. Soc.*, 2020, **142**, 16776–16786.

